The Role of a Novel Auxiliary Pocket in Bacterial Phenylalanyl-tRNA Synthetase Druggability[S]

Ayome Abibi[‡1], Andrew D. Ferguson[§], Paul R. Fleming[¶], Ning Gao[‡], Laurel I. Hajec[‡], Jun Hu[§], Valerie A. Laganas[‡], David C. McKinney[¶], Sarah M. McLeod[‡], D. Bryan Prince[§], Adam B. Shapiro[‡], and Ed T. Buurman[‡2]

From the Departments of [‡]Biosciences and [¶]Chemistry, Infection Innovative Medicines Unit and the [§]Department of Structure and Biophysics, Discovery Sciences, AstraZeneca R&D Boston, Waltham, Massachusetts 02451

Background: Phenylalanyl-tRNA synthetase inhibitors have been shown to be efficacious in animal models of infection.
Results: Inhibitors occupy a newly identified hydrophobic auxiliary binding pocket.
Conclusion: Compound binding in this pocket leads to high screening hit rates, resistance frequencies, and elevated plasma protein binding.
Significance: New inhibitors may be identified by avoiding the auxiliary pocket.

The antimicrobial activity of phenyl-thiazolylurea-sulfon-amides against *Staphylococcus aureus* PheRS are dependent upon phenylalanine levels in the extracellular fluids. Inhibitor efficacy in animal models of infection is substantially diminished by dietary phenylalanine intake, thereby reducing the perceived clinical utility of this inhibitor class. The search for novel antibacterial compounds against Gram-negative pathogens led to a re-evaluation of this phenomenon, which is shown here to be unique to *S. aureus*. Inhibition of macromolecular syntheses and characterization of novel resistance mutations in *Escherichia coli* demonstrate that antimicrobial activity of phenyl-thiazolylurea-sulfonamides is mediated by PheRS inhibition, validating this enzyme as a viable drug discovery target for Gram-negative pathogens. A search for novel inhibitors of PheRS yielded three novel chemical starting points. NMR studies were used to confirm direct target engagement for phenyl-alanine-competitive hits. The crystallographic structure of *Pseudomonas aeruginosa* PheRS defined the binding modes of these hits and revealed an auxiliary hydrophobic pocket that is positioned adjacent to the phenylalanine binding site. Three viable inhibitor-resistant mutants were mapped to this pocket, suggesting that this region is a potential liability for drug discovery.

Protein translation has proven to be a rich source of antibacterial drug discovery targets. An essential step in this process is the aminoacylation of tRNAs. Inhibition of a single aminoacyl tRNA synthetase (aaRS)[3] halts translation or leads to the mis-incorporation of amino acids. The presence of aaRSs among bacterial species varies widely, which limits the potential clinical spectrum of aaRS inhibitors. Complete genome analysis reveals that a full complement of 20 canonical aaRSs is uncommon (1). More often, tRNA-dependent amidotransferases acting on Asp-tRNA and Glu-tRNA compensate for the absence of AsnRS and GlnRS, which narrows the spectrum of AsnRS or GlnRS inhibitors. Conversely, multiple aaRS isozymes can be present among bacterial strains, which also limits the spectrum of an inhibitor to a subset of a population when it acts against only one of these isozymes. For example, one of two MetRS paralogs was identified in different *Streptococcus pneumoniae* strains, yielding subpopulations with differing sensitivities to a tetrahydroquinoline inhibitor (2). A variation on this theme is the occurrence of mupirocin-resistant IleRS isozymes in *Staphylococcus aureus*, MupA and MupB. Although their prevalence was low when the topical IleRS inhibitor mupirocin was launched, their presence has given rise to increased clinical resistance (3). In contrast to these examples, the genes encoding PheRS subunits, *pheS* and *pheT*, have been found in all genomes as single copies, highlighting the potential for an agent with broad spectrum antibacterial activity (1).

aaRSs can be divided into two structural classes, I and II (4), and subdivided into three subclasses (5). This partition is correlated with biochemical differences, including the bound conformation of ATP and tRNA, the location of the aminoacylated hydroxyl group on the terminal ribose of the tRNA, and the formation of either catalytic α-monomers or obligate α_2-homodimers (6).

PheRS is a class II aaRS with an additional β-subunit that forms a $(\alpha\beta)_2$ heterotetramer (7, 8). Unlike other class II aaRSs, PheRS aminoacylates the tRNA at the 2′- and not the 3′-hydroxyl position (9, 10). The smaller catalytic α-subunit PheS (350 residues) catalyzes the initial acyl transfer reaction that converts phenylalanine and ATP into the stable intermediate phenylalanyl-adenylate. Phenylalanine is subsequently transferred to the 3′-end of tRNA$^{\text{Phe}}$ (11). The larger β-subunit PheT (800 residues) mediates the physical interaction with the tRNA$^{\text{Phe}}$ molecule and exclusively carries out the editing func-

---

tion of the enzyme by cleaving tRNA molecules that are mischarged with tyrosine (7, 8, 12).

Eukaryotes contain distinct cytosolic and mitochondrial PheRS homologs. Although the structural architecture of cytosolic PheRS is similar to bacterial PheRS, differences in functionally important residues have been described (13). Mitochondrial PheRS is a monomeric protein that appears to have evolved from an $\alpha\beta$ chimeric protein (14). These structural differences hold promise for the development of selective inhibitors, as demonstrated by the discovery of a wide array of bacterial PheRS inhibitors with broad biochemical spectrum and selectivity against their human counterparts, such as spirocyclic furans and pyrrolidines (15, 16), ethanolamines (17), and benzyl phenyl ethers (18). Unfortunately, the antimicrobial activity of these compounds was marginal.

A significant advance came with the discovery of phenylthiazolylurea-sulfonamides with both antimicrobial activity and reduced organ burdens in sepsis models of *S. aureus* and *S. pneumoniae* in mice (19). Consistent with these compounds acting competitively with substrate, the addition of phenylalanine to the growth medium reduced the *in vitro* antimicrobial potency against *S. aureus.* Subsequent studies showed that phenylalanine blood levels in mice were dependent on their diet, which reduced efficacy in regularly fed mice. Assuming these findings could be extrapolated to humans, the clinical utility of phenylalanine-competitive PheRS inhibitors as antimicrobial agents appeared limited.

Although phenyl-thiazolylurea-sulfonamides inhibitors showed antimicrobial activity against the Gram-negative pathogens *Haemophilus influenzae* and *Moraxella catarrhalis*, and inhibited PheRS isolated from other Gram-negative species, phenylalanine complementation was marginal compared with *S. aureus* (19). This observation suggested that phenylalanine serum levels would not limit the clinical utility of PheRS inhibitors against Gram-negative pathogens or that the cellular target of phenyl-thiazolylurea-sulfonamides differs between Gram-positive and Gram-negative pathogens (20).

The mechanism of growth inhibition in Gram-negative pathogens was investigated through the isolation of resistant mutants. To rationalize the impact of these mutations, the crystal structure of *Pseudomonas aeruginosa* PheRS was determined in complex with four distinct chemical scaffolds. Combined with NMR competition data, these structures were used to define the inhibitor binding mode. In addition, an auxiliary hydrophobic pocket was identified adjacent to the phenylalanine binding pocket into which the inhibitors bind but not phenylalanine. Recognition of this drug discovery liability will be critical for future success in exploitation of this enzyme as an antimicrobial target.

MATERIALS AND METHODS

Strains—*S. pneumoniae* NCTC 7464, *S. aureus* RN4220 (21), *P. aeruginosa* PAO1 (22), *H. influenzae* ATCC 51907, and *Escherichia coli* ATCC27325 were used in this study. Efflux-negative strains *H. influenzae acrB*::cap and *E. coli tolC*::Tn10 and *P. aeruginosa mexABCDXY* were derived as previously described (20, 21).

Determination of Antimicrobial Activity—Antimicrobial activity was determined using CLSI conditions (23) unless oth-

erwise stated. The defined medium used in this study was similar to that described previously (19) and consisted of M9 medium with 0.4% glucose (24) supplemented with 100 μM of all canonical amino acids except phenylalanine.

Inhibition of Macromolecule Biosynthesis—The incorporation of radiolabeled metabolic precursors was performed in *H. influenzae* as described (25, 26), and Mueller Hinton II broth was used for *S. aureus* and *E. coli tolC* instead of haemophilus test medium.

Isolation and Characterization of Resistant Mutants—Resistant mutants of *E. coli tolC* were isolated as described previously (20). Compound **1a** or **1b** was added at 1.6, 3.2, 6.3, and 12.5 μM to Mueller Hinton II agar plates. An inoculum of 10^5 cells was used to determine the agar MIC values, which were 1.6 and 6.3 μM, respectively. Larger inocula of 10^7–10^8 cells yielded resistant colonies at a frequency of 10^{-8}–10^{-7} at 2–4-fold above the agar MIC value. The *pheS* genes of 18 mutants were PCR-amplified and sequenced, leading to the identification of three unique single residue mutations in PheS. These isolates have been deposited in the Yale University *E. coli* Genetic Stock Center.

Aminoacylation Assay—Compounds were solubilized in DMSO. Serial 2-fold dilutions covering two concentration ranges, 10 mM to 19.5 μM and 100 μM to 195 nM, were prepared. 0.6 μl/well of the diluted compound solutions (50× the final assay concentration) were added to white 384-well polystyrene assay plates (Thermo Fisher Scientific/Matrix Technology Corp., Hudson, NH). Uninhibited control wells (MAX) received 2 μl of 30% (v/v) DMSO. Baseline wells (MIN) received 2 μl of a solution containing 30% (v/v) DMSO and 15 mM L-phenylalanine (Sigma-Aldrich). Assays were performed in a buffer consisting of 50 mM Tris-HCl (pH 8.0), 50 mM NH$_4$Cl, 10 mM MgCl$_2$, 2 mM DTT, 0.005% Tween 20 (Surfact-Amps-20, Thermo Fisher Scientific/Pierce Protein Research products, Suwanee, GA), and 0.1 mM EDTA-NaOH (pH 8.0). Compounds were preincubated with 15 μl/well of either 2 nM *E. coli* PheRS, 2 nM *H. influenzae* PheRS, or 0.8 nM *P. aeruginosa* PheRS in buffer for 30 min at 2× final assay concentrations. The reactions were initiated with 15 μl/well of a 2× substrate solution in buffer containing 2 μM *E. coli* phenylalanine tRNA (Sigma-Aldrich), 100 μM ATP, and 2 μM [^{3}H]Phe with a specific radioactivity of 6.3 Ci/mmol (PerkinElmer Life Sciences). The reactions were quenched after 30 min with 15 μl/well of a solution containing 4 mg/ml PVT/PEI/WGA type A SPA beads (PerkinElmer Life Sciences), 262 mM sodium citrate (pH 2.0), and 150 mM NaCl. The plates were sealed with transparent film (PerkinElmer Life Sciences). The beads were allowed to settle for a minimum of 2 h before scintillation counting with a TopCount plate reader (PerkinElmer Life Sciences). [^{3}H] counts (CPM) for aminoacylated tRNA were measured for 1 min/well. The percentage of inhibition was calculated using the equation: % inhibition = 100 × (1 − (CPM − MIN)/(MAX − MIN)), where MAX and MIN are the averages of 32 wells each per plate. Typical values of MIN and MAX were 35 and 720 CPM, respectively.

The IC$_{50}$ values (concentration of inhibitor producing 50% inhibition) were calculated for each compound dilution series by nonlinear least squares regression using the equation: %

inhibition = $100 - [I]^n/(IC_{50} + [I]^n)$ where [I] is the inhibitor concentration, and n is the Hill slope.

PheRS Expression Plasmids—*pheS* and *pheT* genes were PCR-amplified and ligated using the pET-46 EK/LIC Cloning Kit with the LIC Duet Minimal Adaptor as described by the manufacturer (EMD Millipore, Billerica, MA). This system brings *pheS* and *pheT* expression under the control of the T7*lac* promoter encoded within the expression plasmid pETDuet-1. All oligonucleotides were custom synthesized (Eurofins MWG Operon, Huntsville, AL). Plasmid pSMM84 encodes truncated forms of *P. aeruginosa* PheS and PheT, expressing residues 80–338 of PheS with an N-terminal His$_6$ tag cloned into the SacI and SalI sites, while encoding residues 1–791 of PheT cloned into the NdeI and KpnI sites. Plasmid pSMM107 expresses a full-length N-terminal His$_6$-tagged PheS and a full-length PheT from *P. aeruginosa*. The reverse PCR primer for the C-terminal end of *pheS* used for construction of pSMM107 encodes two additional stop codons to prevent readthrough. Plasmids pLH1504 and pLH1514 were cloned as described for pSMM107. Plasmid pLH1504 expresses full-length His$_6$-tagged PheS and full-length PheT from *H. influenzae*, whereas plasmid pLH1514 expresses full-length His$_6$-tagged PheS and full-length PheT from *E. coli*.

PheRS Overexpression—*E. coli* BL21(DE3) (Invitrogen) was transformed with plasmid pSMM84, plated on LB agar containing 100 μg/ml ampicillin (Sigma-Aldrich), and grown overnight at 37 °C. A single transformant was inoculated into a 100-ml starter culture of LB broth containing 100 μg/ml ampicillin and grown overnight at 37 °C. The overnight culture was diluted to an initial A_{600} of 0.1 in four 1-liter cultures and grown at 37 °C with aeration until the A_{600} reached 0.3. The cultures were then transferred to 16 °C and grown until the A_{600} reached 0.6, at which point isopropyl β-D-thiogalactopyranoside (Acros Organics) was added to a final concentration of 0.3 mM and grown overnight. The cells were harvested by centrifugation at 5,000 × g for 15 min at 25 °C and frozen. Overexpression of PheRS using plasmids pSMM107, pLH1504, and pLH1514 were performed as described with the following modifications. Plasmid pSMM107 was transformed into *E. coli* HMS174(DE3) (EMD Millipore) and grown at 30 °C until the A_{600} reached 0.5, and induction was performed at room temperature overnight. Plasmids pLH1504 and pLH1514 were transformed into *E. coli* BL21(DE3)pLysS (EMD Millipore) and were grown at 30 °C until the A_{600} reached 0.5. Expression from the pLH1504 plasmid was induced at room temperature overnight, whereas the pLH1514 plasmid was induced at 30 °C for 4.5 h at room temperature.

PheRS Purification—Cell pellets were suspended in 50 ml of lysis buffer consisting of Buffer A (25 mM Tris-HCl, pH 8.0, 0.3 M NaCl, 5% glycerol) and one EDTA-free Protease inhibitor mixture tablet (Roche Molecular Biochemical). Use of a French press at 18,000 p.s.i. twice at 4 °C disrupted cells, and the crude extract was centrifuged at 150,000 × g for 30 min at 4 °C. The clarified supernatant was applied to a HiTrap Ni^{2+} chelating column (GE Healthcare) pre-equilibrated with Buffer A. The column was washed with Buffer A, and the PheRS complex was eluted using a linear imidazole gradient in Buffer A. Fractions containing the PheRS complex were pooled and characterized

by SDS-PAGE and analytical LC-MS. The purified protein was stored at −80 °C.

The N-terminal His$_6$ tag was proteolytically removed from the truncated PheRS complex (residues 80–338 of PheS with an N-terminal His$_6$ tag and residues 1–791 of untagged PheT) for crystallization. Specifically, thrombin (EMD Millipore) was added to the pooled fractions and dialyzed against 1 liter of 25 mM Tris-HCl (pH 8.0), 0.1 M NaCl, and 5% glycerol at 4 °C overnight. The dialyzed sample was then reapplied to a HiTrap Ni^{2+} chelating column pre-equilibrated with Buffer A. The fractions containing the PheRS complex were pooled and concentrated using an Amicon Ultracell-10K filtration concentrator (EMD Millipore). The concentrated sample was further purified by size exclusion chromatography using a Sephacryl S300 (HR 26/60) column (GE Healthcare) pre-equilibrated with Buffer B (25 mM Tris-HCl, pH 8.0, 1 mM DTT, 1 mM EDTA, 10% glycerol and 150 mM NaCl). Fractions containing the PheRS complex were pooled and characterized by SDS-PAGE and analytical LC-MS. The observed molecular masses were 29,418 Da for PheS (expected 29,419 Da) and 86,671 Da for PheT (expected 86,672 Da). Purified protein was concentrated to 25 mg/ml and stored at −80 °C.

Protein Engineering—The rational protein engineering approach applied by Evdokimov *et al.* (27) for *Staphylococcus haemolyticus* PheRS was utilized to engineer the *P. aeruginosa* PheRS complex for crystallographic studies. Briefly, a variety of full-length and N-terminal truncation constructs were designed to remove expected regions of disorder within PheS and to introduce a series of surface entropy reduction mutations within PheT to eliminate the formation of inefficient crystal contacts that would lead to low resolution and/or anisotropic diffraction and irreproducible crystallization. A structure-based protein sequence alignment of *P. aeruginosa*, *S. haemolyticus*, *E. coli*, and *T. thermophilus* PheRS was used to visualize the expected impact of the truncation and mutagenesis strategy. From these efforts, a bicistronic expression plasmid encoding residues 80–338 of PheS with a cleavable N-terminal His$_6$ tag and residues 1–791 of untagged PheT was constructed. The N-terminal His$_6$ tag was proteolytically cleaved with thrombin prior to crystallization studies to minimize the disorder of the N terminus of PheS. Using this truncated protein, crystallization screening identified initial crystal growth conditions that were extensively optimized, followed by the development of a suitable cryoprotection protocol.

Crystallography—All x-ray diffraction data were collected at cryogenic temperature using synchrotron radiation at Beamlines ID-17 and ID-24 at the Advance Photon Source. Diffraction data collected at IMCA-CAT was processed with XDS (28) and scaled using SCALA (29), as implemented in the auto-PROC routines from Global Phasing (30). Diffraction data collected at NE-CAT were processed using HKL2000 (31). These crystals belong to the monoclinic space group *C*2, contain two PheRS heterodimers per asymmetric unit, and have a Mat-thews' coefficient of 2.87 Å^3/Da (corresponding to an estimated solvent content of 57%) (supplemental Table S1).

The structure of apo PheRS from *P. aeruginosa* was solved at 2.79 Å resolution by molecular replacement using the program MOLREP with the coordinates of PheRS from *S. haemolyticus*

TABLE 1

Antimicrobial activity of phenyl-thiazole-sulfonamide PheRS inhibitors

Antimicrobial activity of phenyl-thiazole-sulfonamide PheRS inhibitors expressed as MICs (μM) were determined under CLSI conditions against *S. aureus* (Sau), *S. pneumoniae* (Spn), *H. influenzae* (Hin), *H. influenzae acrB*::cap (Hin*), *E. coli tolC*::Tn10 (Eco*), and *P. aeruginosa mexABCDXY* (Pae*). No activity (>100 μM) was observed against wild-type strains of *E. coli* and *P. aeruginosa*. Antimicrobial activity against Sau, Eco*, and Pae* were determined in defined medium in the presence and absence of 100 μM phenylalanine.

	CLSI						Defined medium (+100 μM Phe)		
	Sau	Spn	Hin	Hin*	Eco*	Pae*	Sau	Eco*	Pae*
1a	>100	50	6.25	0.78	3.1	>100	12.5 (>50)	0.4 (0.8)	>100 (>100)
1b	50	50	12.5	1.56	6.3	100	1.6 (25)	3.1 (6.2)	50 (50)

(Protein Data Bank accession code 2RHQ) as the search model (27, 32). The structures of all liganded PheRS complexes were subsequently determined using the coordinates of the apo structure. Examination of the electron density maps for all liganded complexes showed clear unambiguous difference density with the expected molecular features of the compound (supplemental Fig. S1). Sequential rounds of manual rebuilding using Coot (33) and refinement using autoBUSTER with TLS, NCS, and target restraints (34), produced models for apo and liganded PheRS complexes. The final refinement statistics are shown in supplemental Table S1. All figures were prepared using PyMOL (Schrödinger). The coordinates and structure factors have been deposited with the Protein Data Bank with accession codes 4P71, 4P72, 4P73, 4P74, and 4P75.

NMR Binding Studies—All NMR spectra were acquired at 298 K with a 600 MHz NMR instrument (Bruker, Billerica MA) with an AVANCE III console and a triple-resonance cryogenic probe. In the WaterLOGSY experiments (35), the first water-selective 180° Sinc pulse was 6 ms long, and a weak rectangular pulse field gradient was applied during the mixing time (1.8 s). A gradient recovery time of 2 ms was introduced after the mixing time. Water suppression was achieved by the excitation sculpting scheme (36) and the water-selective 180° Sinc shape pulse was 3 ms long. The data were collected with a sweep width of 9157 Hz, 0.45-s acquisition time, and 1.8 s for the relaxation delay. For each experiment 128 scans were recorded, requiring 9 min/spectrum. The data were zero-filled to 32,768 complex points and multiplied by an exponential function (line broadening, 3 Hz) prior to Fourier transformation.

Chemistry—Synthesis of compounds was performed in house and is described in the supplemental information. Compound purity was determined by LC/MS shortly before biological testing and was >90%.

Physicochemical Properties—Plasma protein binding and logD$_{7.4}$ determinations were performed as described (37). Equilibrium solubility was measured according established methods (38).

RESULTS

Phenyl-thiazolylurea-sulfonamides act via PheRS in Gram-negative Species—The antimicrobial activity of two representative phenyl-thiazolylurea-sulfonamides, compounds **1a** and **1b** (19), were evaluated under CLSI conditions (23). Despite limited compound solubility under these conditions (50–200 μM), MIC values were determined (Table 1). The addition of 100 μM phenylalanine did not increase the observed MIC values for any of the evaluated bacterial strains because these media contain 2 mM phenylalanine. An equivalent experiment was performed
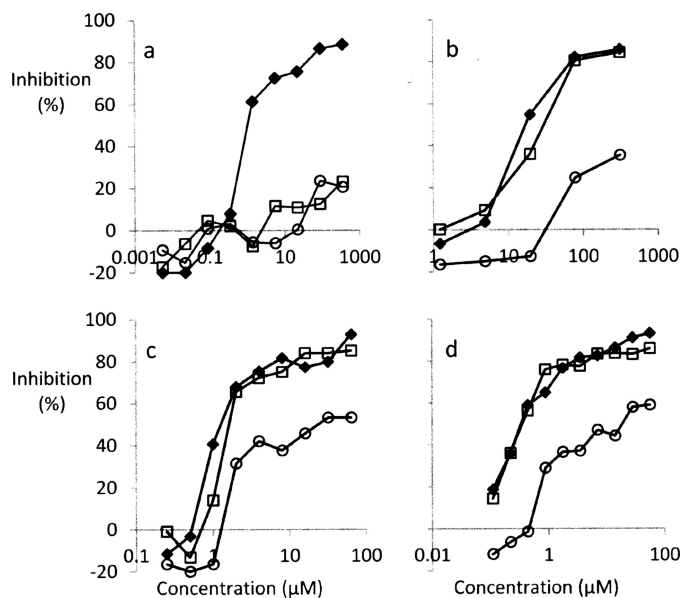

FIGURE 1. **Compound 1a preferentially inhibits leucine and uridine incorporation into macromolecules of *E. coli tolC*, followed by thymidine incorporation.** Protein synthesis inhibition (leucine incorporation; *black diamonds*), RNA (uridine incorporation; *white squares*), and DNA (thymidine incorporation; *white circles*) were measured as described under "Materials and Methods." The incorporation rates of added precursors into uninhibited cells were 13, 282, and 9 μmol/h/A_{600}, respectively. *a*, erythromycin; *b*, rifampin; *c*, mupirocin; *d*, compound **1a**.

using defined minimal salts medium. The results showed increased MIC values following the addition of phenylalanine for *S. aureus* only, whereas the MIC values for *E. coli tolC* and *P. aeruginosa mexABCDXY* remained constant. Taken together, these results are consistent with the previously described phenylalanine complementation data for *S. aureus* PheRS (19).

To determine whether an alternative mechanism of growth inhibition could be utilized by Gram-negative pathogens, radiolabeled precursor incorporation studies were conducted in the presence of compound **1a**. Whereas the translation inhibitor erythromycin showed selective inhibition of protein synthesis (Fig. 1*a*), mupirocin (Fig. 1*c*) and compound **1a** (Fig. 1*d*) showed concomitant inhibition of RNA synthesis with weaker inhibition of DNA synthesis. This incorporation pattern is similar to that caused by the RNA polymerase inhibitor rifampin (Fig. 1*b*) and is consistent with the inhibition of RNA polymerase upon binding of (p)ppGpp following binding of uncharged tRNA^{Phe} to the ribosomal A-site as part of the stringent response (39, 40). Similar effects were observed in *S. aureus* (Fig. 2, *a–d*) and *H. influenzae* (data not shown).

To confirm direct target engagement of compound **1a** with PheRS, resistant mutants of *E. coli tolC* were isolated at a fre-
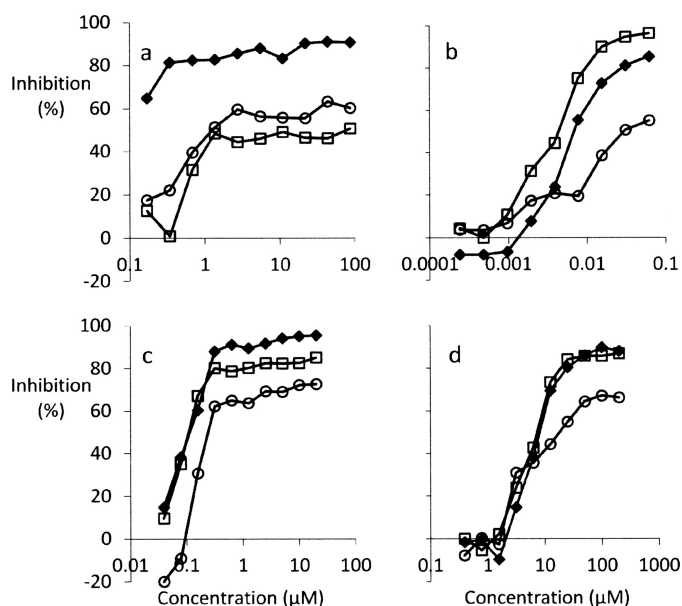
FIGURE 2. **Compound 1a preferentially inhibits leucine and uridine incorporation into macromolecules of *S. aureus*, followed by thymidine incorporation.** Protein synthesis inhibition (leucine incorporation; *black diamonds*), RNA (uridine incorporation; *white squares*), and DNA (thymidine incorporation; *white circles*) were measured as described under "Materials and Methods." The incorporation rates of added precursors into uninhibited cells were 27, 3400, and 67 μmol/h/A_{600}, respectively. *a*, erythromycin; *b*, rifampin; *c*, mupirocin; *d*, compound **1a**.

quency of 10^{-8}–10^{-7} when selected at compound concentrations in agar plates that were 2–4-fold higher than the MIC values of the parental strain. A total of 18 mutant strains were isolated that all contained a single residue mutation in PheS: A189E, V275E, or V279E, corresponding to residues Cys-110, Val-207, and Val-211 of *P. aeruginosa* PheS (supplemental Fig. S1). Under CLSI conditions, these mutations increased the MIC values of compound **1a** from 3.1 to 100 μM for all three resistance mutants and from 6.3 to 25 for the A189E mutation, to 100 μM for the V275E mutation and to 25 μM for the V279E mutation for compound **1b** (supplemental Table S2). Taken together, these results demonstrated that the antimicrobial activity of compounds **1a** and **1b** was mediated by PheRS inhibition.

To confirm the enzymatic inhibition of PheRS, aminoacylation assays were performed using purified PheRS from *E. coli*, *H. influenzae*, and *P. aeruginosa*. Under optimized assay conditions and in agreement with previous reports (19, 41), the $K_{m, \text{app}}$ values of phenylalanine, ATP, and tRNA$^{\text{Phe}}$ of *E. coli* PheRS were determined to be 1.4, 93, and 0.3 μM. Although these compounds are nanomolar inhibitors of these PheRS isozymes, the biochemical IC$_{50}$ values against *P. aeruginosa* PheRS were about 10-fold higher than those against *E. coli* (Table 2) and *H. influenzae* PheRS (data not shown). We attribute these differences to sequence similarities (but not identities) within the inhibitor binding site of these isozymes (supplemental Fig. S1).

Crystal Structure of P. aeruginosa PheRS—A variety of PheRS crystal structures from *E. coli* and *Thermus thermophilus* have been previously described, including the apo enzyme, complexes with either tRNA$^{\text{Phe}}$ or the substrates phenylalanine and AMP, and with the phenylalanyl-adenylate intermediate (12,

42–44). Moreover, two PheRS structures from the Gram-positive pathogen *S. haemolyticus* with a phenyl-thiazolylurea-sulfonamide inhibitor (compound **1a**) have been determined (27). To understand the structure-activity relationships of published inhibitors and to facilitate the structure-guided design of novel antibacterial compounds, the crystal structure of the PheRS complex from the Gram-negative pathogen *P. aeruginosa* was solved.

The architecture of the *P. aeruginosa* $(\alpha\beta)_2$ heterotetramer is consistent with previously described bacterial PheRS structures (Fig. 3). The smaller component of the heterotetramer, PheS, consists of a central globular domain and a N-terminal extension that forms supplemental interactions with PheT and the tRNA$^{\text{Phe}}$ molecule. PheS from *P. aeruginosa* is most structurally homologous to PheS from the engineered form of *S. haemolyticus* (RMSD of 1.07 Å of 229 aligned residues; sequence identity of 55%), PheS from *E. coli* (RMSD of 1.17 Å over 224 aligned residues; sequence identity of 70%), and PheS from *T. thermophilus* (RMSD of 1.33 Å over 219 aligned residues; sequence identity of 53%).

The larger component of the $(\alpha\beta)_2$ heterotetramer, PheT, is composed of four globular domains, two of which do not form any contacts with PheS and exclusively mediate interactions with the tRNA$^{\text{Phe}}$ molecule. PheT from *P. aeruginosa* shows the highest level of structural homology with PheT from *E. coli* (RMSD of 2.31 Å over 705 aligned residues; sequence identity of 45%), PheT from the engineered form of *S. haemolyticus* (RMSD of 2.65 Å of 716 aligned residues; sequence identity of 30%), and PheT from *T. thermophilus* (RMSD of 2.38 Å over 638 aligned residues; sequence identity of 36%).

The Phenylalanyl-adenylate Binding Site—The phenylalanyl-adenylate binding pocket of *P. aeruginosa* PheRS is composed exclusively of residues from PheS. The crystal structure of *E. coli* PheRS in complex with AMP and phenylalanine previously defined the positions of these substrates within the binding pocket (42). In comparing the *E. coli* structure to the apo structure of *P. aeruginosa* PheRS, all residues that are expected to interact with the phenylalanine or AMP substrates are invariant between these isozymes, except for residue His-90, which stabilizes the carbonyl oxygen of the phenylalanine molecule at the base of the binding pocket (Fig. 4*a*). The crystal structure of PheRS from *T. thermophilus* in complex with a phenylalanyl-adenylate analog (44) further defines the scope of the pocket and its shape similarity to the *P. aeruginosa* enzyme. A sequence alignment of Gram-positive and Gram-negative PheRS isozymes, highlighting residue sequence conservation in PheS, is presented in supplemental Fig. S1.
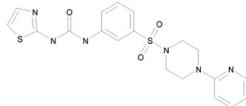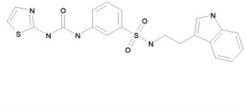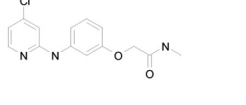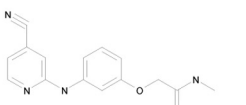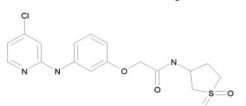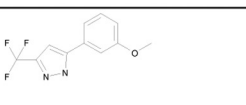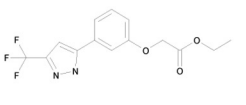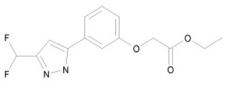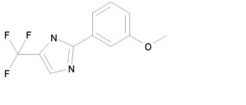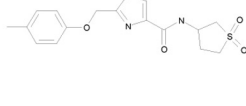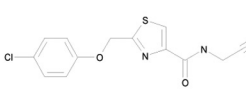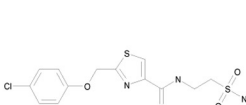
Phenyl-thiazolylurea-sulfonamides—The structure of compound **1a** in complex with *P. aeruginosa* PheRS was solved at 3.03 Å resolution (supplemental Table S1 and Fig. S2*a*). Comparisons to the liganded *S. haemolyticus* enzyme (27) showed nearly perfect superposition within the binding site. Although the phenyl-sulfonamide core occupies a similar position within the binding site as phenylalanine, the thiazolylurea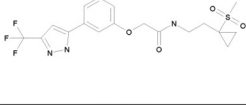 component extends much deeper into an auxiliary hydrophobic pocket (Fig. 4*b*). This auxiliary hydrophobic pocket is located below the bound phenylalanine in the *E. coli* PheRS structure. Two hydrogen bonds are formed between the urea and side chain of

TABLE 2

Biochemical potency, antimicrobial activity and physicochemical properties of PheRS inhibitors

IC_{50} values are expressed in μM and were determined against the isozymes from *E. coli* and *P. aeruginosa*. MIC values determined under CLSI conditions are expressed in μM and were determined against *H. influenzae acrB*::cap (Hin*), *E. coli tolC*::Tn10 (Eco*), and *P. aeruginosa mexABCDXY* (Pae*). The activity against parental strains is indicated in parentheses.

		IC_{50} (μM)		MIC (μM)			Physicochemical properties[a]
Compound		Eco	Pae	Hin*	Eco*	Pae*	
1a		0.0027	0.022	0.8 (25)	1.6 (>200)	200 (>200)	$LogD_{7.4}$: 3.2 Eq sol (μM): 2 $F_{u, hu}$ (%): <1
1b		0.0022	0.013	1.6 (50)	3.1 (>200)	>200 (>200)	$LogD_{7.4}$: >3.5 Eq sol (μM): 16 $F_{u, hu}$ (%): <1
2a		1.4	82	50 (200)	200 (>200)	>200 (>200)	$LogD_{7.4}$: 2.5 Eq sol (μM): 52 $F_{u, hu}$ (%): 6.7
2b		0.56	41	200 (>200)	>200 (>200)	>200 (>200)	$LogD_{7.4}$: 1.9 Eq sol (μM): 97 $F_{u, hu}$ (%): 31
2c		0.1	34	100 (>200)	200 (>200)	>200 (>200)	$LogD_{7.4}$: 2.2 Eq sol (μM): 23 $F_{u, hu}$ (%): 10
3a		0.06	10	100 (200)	200 (>200)	>200 (>200)	$LogD_{7.4}$: 2.5 Eq sol (μM): 208 $F_{u, hu}$ (%): 2.4
3b		0.08	11	n.d. (>200)	>200 (>200)	>200 (>200)	$LogD_{7.4}$: 3.2 Eq sol (μM): 82 $F_{u, hu}$ (%): 11
3c		1.0	59	100 (>200)	>200 (>200)	>200 (>200)	$LogD_{7.4}$: 2.3 Eq sol (μM): 84 $F_{u, hu}$ (%): n.d.
3d		16	>200	100 (>200)	>200 (>200)	>200 (>200)	$LogD_{7.4}$: n.d. Eq sol (μM): 64 $F_{u, hu}$ (%): 7.1
3e		0.07	4.2	>200 (>200)	>200 (>200)	>200 (>200)	$LogD_{7.4}$: 2.8 Eq sol (μM): 3.5 $F_{u, hu}$ (%): 11
4a		1.4	80	200 (>200)	>200 (>200)	>200 (>200)	$LogD_{7.4}$: 2.2 Eq sol (μM): 84 $F_{u, hu}$ (%): 15
4b		0.10	13	n.d. (50)	>200 (>200)	>200 (>200)	$LogD_{7.4}$: 2.1 Eq sol (μM): 55 $F_{u, hu}$ (%): 5.9
4c		0.19	26	100 (>200)	>200 (>200)	>200 (>200)	$LogD_{7.4}$: 2.4 Eq sol (μM): 39 $F_{u, hu}$ (%): n.d.

[a] Eq sol, equilibrium solubility; $F_{u,hu}$, human serum unbound fraction; n.d., not determined.
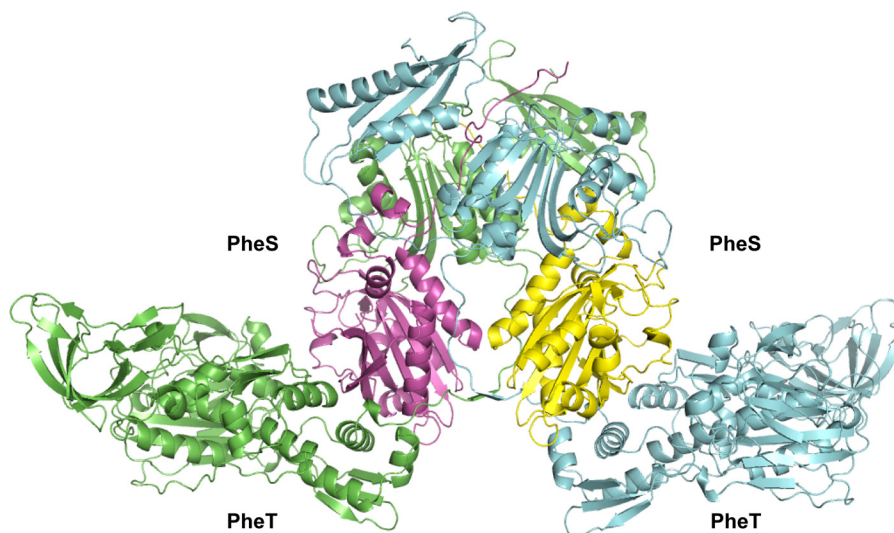
FIGURE 3. **Crystal structure of the *P. aeruginosa* PheRS complex.** The $(\alpha\beta)_2$ heterotetramer is shown with PheS colored *magenta* and *yellow* and PheT colored *green* and *blue*.

residue Glu-131, and another is formed between the side chain of residue Gln-95 and the thiazole ring (Fig. 5*a*). The sulfonamide oxygen forms a water-mediated interaction with the side chain of residue Gln-129 and the main chain amide of residue Gly-203. However, the piperazine substituent of compound **1a** does not form any electrostatic interactions, nor does it overlap with the AMP molecule.

Search for Novel Inhibitory Scaffolds—Although the phenyl-thiazolylurea-sulfonamides showed sufficient cellular activity to determine efficacy in animal models of infection (19), their low aqueous solubility (2 μM) and plasma protein binding of >99% (Table 2) could make formulation of an intravenous clinical product challenging and the dosage high. An attempt was made to identify alternative chemical scaffolds with more attractive physicochemical properties, in particular, those with a lower lipophilicity ($\log D_{7.4}$). High throughput screening of the corporate compound library yielded many hits. Three novel scaffolds passed our selection criterion of calculated lipophilicity ($\text{clog}D_{7.4}$) <3 and were resynthesized and pursued.

Pyridinyl Anilines—A series of pyridinyl anilines were synthesized, and the crystal structure of *P. aeruginosa* PheRS in complex with compound **2a** was determined at 2.62 Å resolution (supplemental Table S1 and Fig. S2*b*). The structure shows that the aniline-linked chloropyridyl forms a single hydrogen bond with the side chain of residue Glu-131 in contrast to the multiple hydrogen bonds of the phenyl-thiazolylurea-sulfonamide **1a** (Fig. 5, *a* and *b*). As observed with the thiazolylurea of compound **1a**, the aniline-linked chloropyridyl group is positioned in the auxiliary hydrophobic pocket. NMR binding studies were used to confirm that the binding of this compound to *P. aeruginosa* PheRS was competitive with the phenylalanine substrate (Fig. 6). Substitution of the lipophilic chlorine with a more polar cyano moiety (compound **2b**) produced a small enhancement in the inhibition of both *E. coli* and *P. aeruginosa* PheRS, a significant reduction in $\log D_{7.4}$, and concomitant improvements in solubility and protein binding (Table 2).

A wider set of amides was synthesized to potentially form additional electrostatic interactions with residues lining the AMP binding pocket. As shown by **2c**, although desirable physicochemical properties were maintained, only modest gains in potency were achieved. These results suggest that within this series, few, if any, additional binding interactions within the AMP binding pocket were established.

Trifluoromethyl Pyrazoles—The structure of compound **3a**, an exemplar trifluoromethyl pyrazole, was determined at 2.96 Å resolution (supplemental Table S1 and Fig. S2*c*). The liganded structure demonstrates that the pyrazole ring forms electrostatic interactions with the side chains of residues Gln-95 and Glu-131 (Fig. 5*c*). Analogous to the thiazolylurea of **1a**, the CF$_3$ substituent is located in the auxiliary hydrophobic pocket of PheRS. The methoxyphenyl group extends toward the bottom of the AMP binding site, and the methoxy substituent is located near the position of the sulfonamide of compound **1a**. NMR binding studies confirmed that this compound is competitive with the phenylalanine substrate (Fig. 6).

The structure-activity relationship of pyrazole ring substitutions revealed the importance of the CF$_3$ group. Removing one of three fluorines (**3c**) decreased the biochemical potency significantly (Table 2). Changing the position of the nitrogen to the isomeric trifluoromethyl imidazole (**3d** *versus* **3a**) rendered this analog inactive. Taken together, these data indicate that the strength of the electrostatic interaction formed between the pyrazole NH and the side chains residues Gln-95 and Gly-131 is important to maintain enzyme inhibition. Attempts to homologate the methoxy group were also pursued. However, as observed with **3e**, only marginal improvements in potency and physicochemical properties were achieved.

Thiazole Amides—The crystal structure of *P. aeruginosa* PheRS with the thiazole amide compound **4a** was also determined at 2.70 Å resolution (supplemental Table S1 and Fig. S2*d*). Competition with phenylalanine was confirmed by NMR binding experiments (Fig. 6). The ether-linked methylphenyl group overlaps with the position of the phenyl-thiazolylurea of **1a**, within the auxiliary hydrophobic pocket, and the ether oxy-
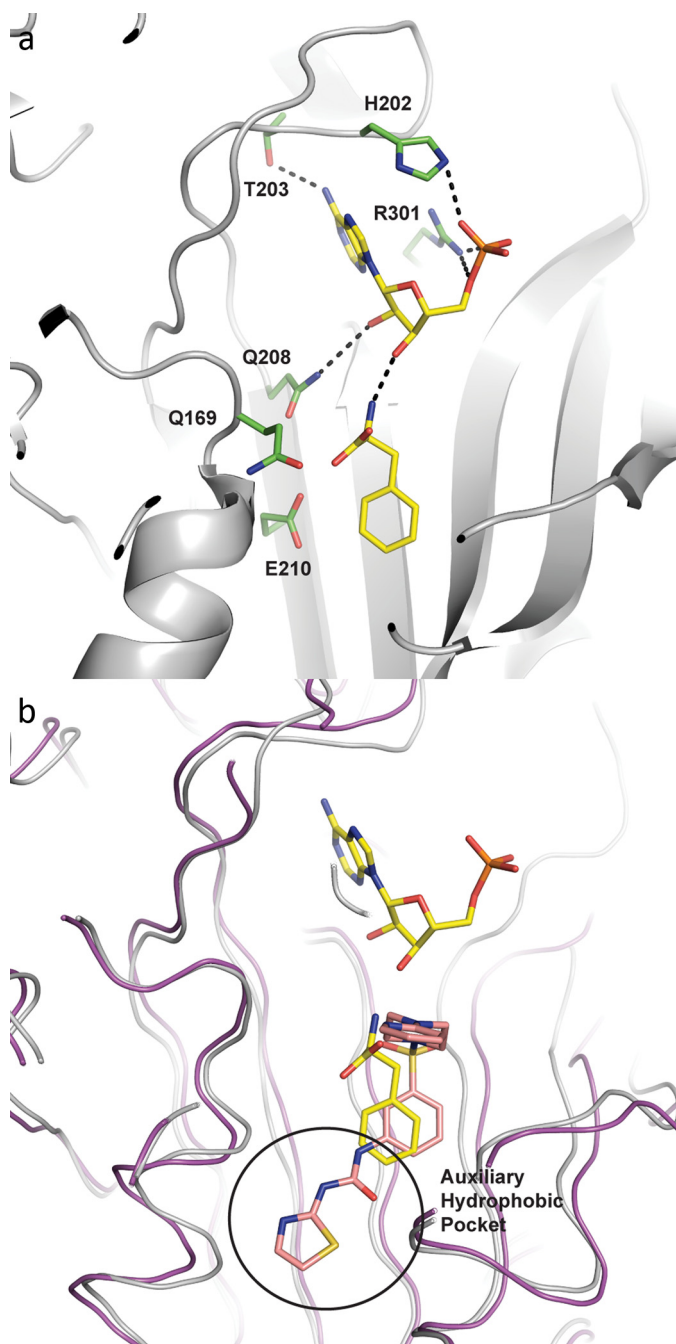
FIGURE 4. **The AMP and phenylalanine binding sites.** *a*, the substrate binding sites for AMP and phenylalanine are shown. The *E. coli* PheRS structure (Protein Data Bank accession code 3PCO) is shown in *white*. The bound substrates are shown as stick models with *yellow* carbon atoms, *red* oxygen atoms, and *blue* nitrogen atoms. Those residues that form electrostatic interactions with either substrate are shown as *green sticks* and labeled, and hydrogen bonds are depicted as *black dotted lines*. *b*, superposition of *P. aeruginosa* PheRS in complex with compound 1a (*magenta*) and *E. coli* PheRS in complex with AMP and phenylalanine (*white*). The bound substrates are shown with *yellow* carbon atoms, *red* oxygen atoms, and *blue* nitrogen atoms. Compound 1a is shown with *pink* carbon atoms, *blue* nitrogen atoms, *red* oxygen atoms, and *yellow* sulfur atoms. The auxiliary hydrophobic pocket is indicated.

gen is placed at the same location as the oxygen from the urea linker (Fig. 5*d*). However, unlike the urea linker, which forms hydrogen bonds with the side chain of residue Glu-131, no specific electrostatic interactions are observed with the ether

oxygen. The thiazole core of **4a** is perfectly superimposed on the phenyl ring of **1a**. In addition, the amide-linked alkyl sulfone forms a hydrogen donor acceptor interaction with the side chain of residue Gln-129 and the backbone amide of residue Gly-230. The alkyl substituent is positioned near the location of the ribose of the AMP substrate.

Thiazole amides such as **4a**, with a non-phenyl group at their core, fill the hydrophobic pocket with a phenyl ether and point an amide toward the remainder of the binding site. Although substitution of the methyl phenol with the slightly more lipophilic chlorophenol results in improved activity, introduction of polar substituents in this region proved deleterious (data not shown). Modification of the amine portion of these amides resulted in significant improvements in potency as exemplified by the cyano methyl (**4b**) and sulfonamidomethyl (**4c**). The addition of these groups should make the amide significantly more acidic and offers the possibility of forming an additional hydrogen bond with the enzyme.

DISCUSSION

Target-based antibacterial discovery aims to convert biochemical inhibitors into efficacious clinical candidates. The first step in this process is to chemically modify the inhibitor to maximize antimicrobial activity. For this strategy to succeed, it is critical that the desired intracellular mechanism of growth inhibition is validated for the structure-activity relationships to be meaningful. aaRSs are among the first antibacterial target classes to be pursued in this manner. The litmus test to verify the intracellular inhibition of an aaRS has been the addition of the relevant amino acid to the growth medium (45). Only those inhibitors that are competitive with the amino acid substrate should reduce antibacterial activity.

Although this premise is true for phenyl-thiazolylurea-sulfonamide inhibitors of *S. aureus* PheRS, reduction of antibacterial activity was not observed in *E. coli, P. aeruginosa* (Table 1), *S. pneumoniae, M. catarrhalis,* or *H. influenzae* (19). As part of this work, phenyl-thiazolylurea-sulfonamide-resistant mutants of *E. coli* were isolated with single residue PheS mutations, indicating that antibacterial activity is driven by the inhibition of its catalytic activity. Differences in phenylalanine complementation against identical PheRS inhibitors likely reflect the presence of distinct phenylalanine uptake mechanisms between *S. aureus* and Gram-negative pathogens. This is a key finding for drug discovery because Beyer *et al.* (19) linked variations in serum phenylalanine concentrations to efficacy changes of PheRS inhibitors in animal models of *S. aureus* infection, leading to the deprioritization of PheRS as an antibacterial target. Our results predict that efficacy against Gram-negative pathogens will be independent from dietary phenylalanine, thereby restoring the clinical promise for PheRS inhibitors.

Although phenyl-thiazole-sulfonamides have been shown to be efficacious, their low aqueous solubility and high serum protein binding make it difficult to calculate tissue exposure levels and predict animal efficacy. Alternative less hydrophobic chemical scaffolds were sought by screening the corporate compound collection. Consistent with previous studies (46), PheRS inhibitors were straightforward to obtain. X-ray crystal-
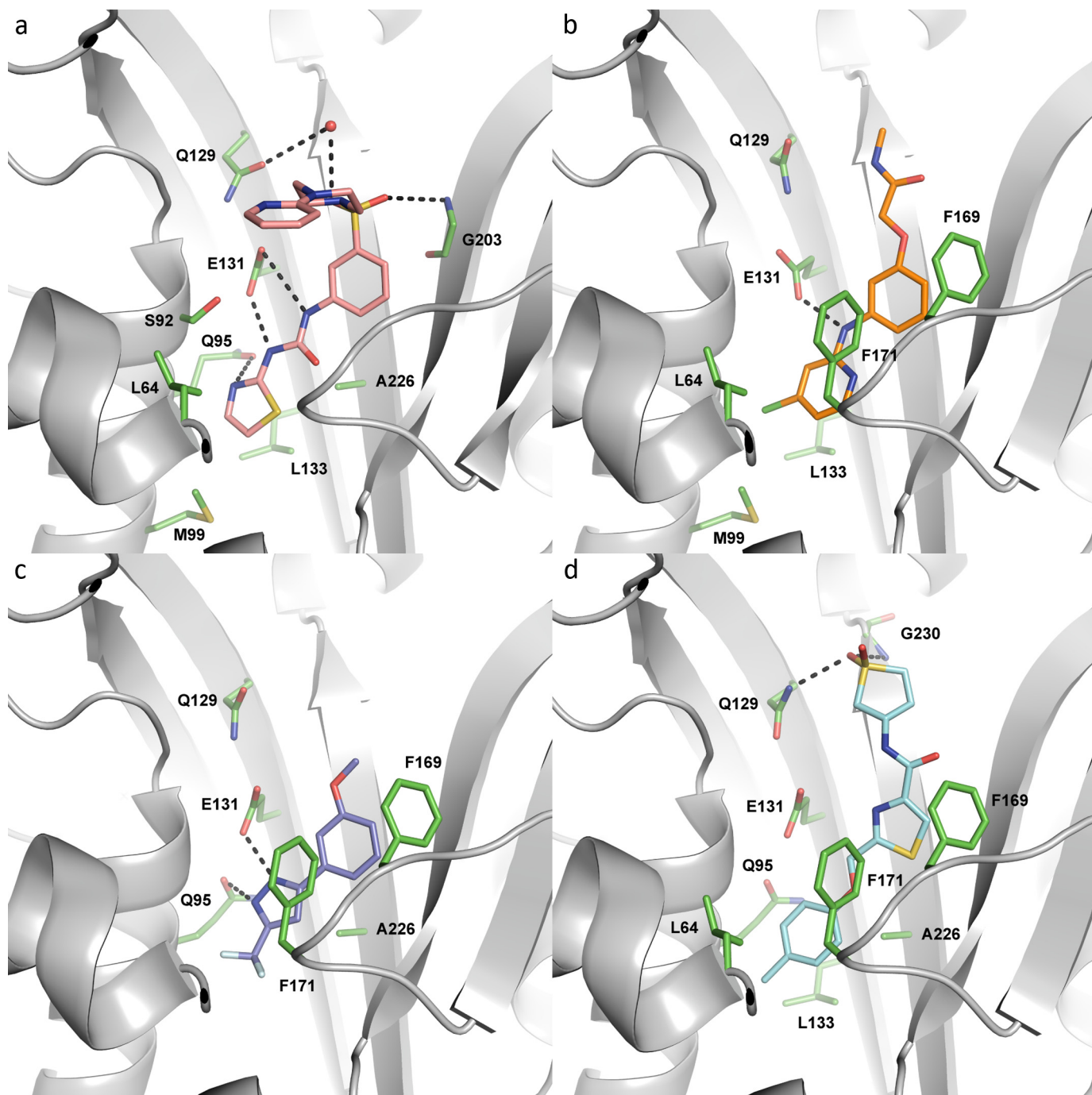
FIGURE 5. **Inhibitor binding sites.** *a*, compound **1a**; *b*, compound **2a**; *c*, compound **3a**; *d*, compound **4a**. *P. aeruginosa* PheRS is shown in *white*, and all residues within 3.5 of the bound inhibitor are shown as *green sticks* and labeled. Hydrogen bonds formed between the inhibitor and PheS residues are depicted as *black dashed lines*. The inhibitors are shown with *red* oxygen atoms, *blue* nitrogen atoms, *yellow* sulfur atoms, and *green* chlorine atoms, and the carbon atoms vary among the inhibitors. Water molecules are shown as *red spheres*.

lography using *P. aeruginosa* PheRS combined with NMR binding studies were used to show that these inhibitors bind in the phenylalanine binding pocket of PheRS and extend into the auxiliary hydrophobic pocket (Figs. 4–6). Structure-guided design was used to improve the physicochemical properties of these inhibitors by extending into the more hydrophilic AMP-binding pocket, producing compounds with improved aqueous solubility and lower protein binding. Although exploration of three distinct chemical scaffolds afforded different vectors to

extend into the AMP-binding pocket, the resulting biochemical potencies did not improve significantly.

The isolation of three *E. coli* resistant mutants provided valuable insights. When viewed in light of the structure of *P. aeruginosa* PheRS with compound **1a**, residues Val-207 and Val-211 are positioned at the base of the phenylalanyl-adenylate binding pocket and are in close proximity to the thiazole ring (Figs. 5*a* and 7). The *E. coli* resistance mutants, V275E and V279E (corresponding to residues Val-207 and Val-211 in the
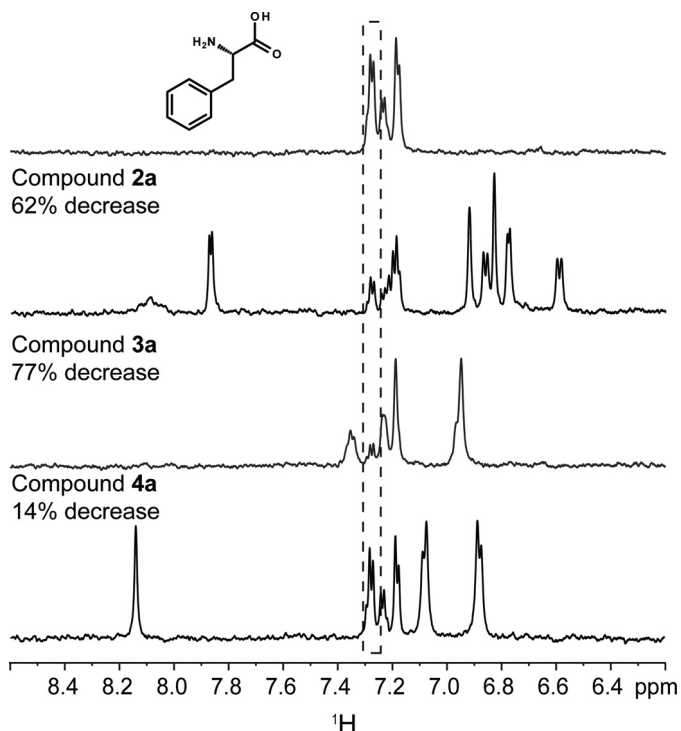
FIGURE 6. **New scaffolds prevent binding of phenylalanine to *P. aeruginosa* PheRS.** One-dimensional WaterLOGSY spectral comparison of 200 μM phenylalanine binding to 10 μM *P. aeruginosa* PheRS in the absence (*top spectrum*) and presence of 200 μM compounds **2a**, **3a**, or **4a**. Signals of two protons (7.25–7.32 ppm) from the phenyl ring on phenylalanine are *boxed* in *dashed lines* and compared in the WaterLOGSY spectra. Signal decrease indicates displacement of phenylalanine by the compound. The NMR samples were prepared in 50 mM HEPES (pH 7.5), 5 mM MgCl$_2$, 5 mM DTT, 0.1 mM EDTA, and 5% deuterated water. The spectra were acquired at 298 K.
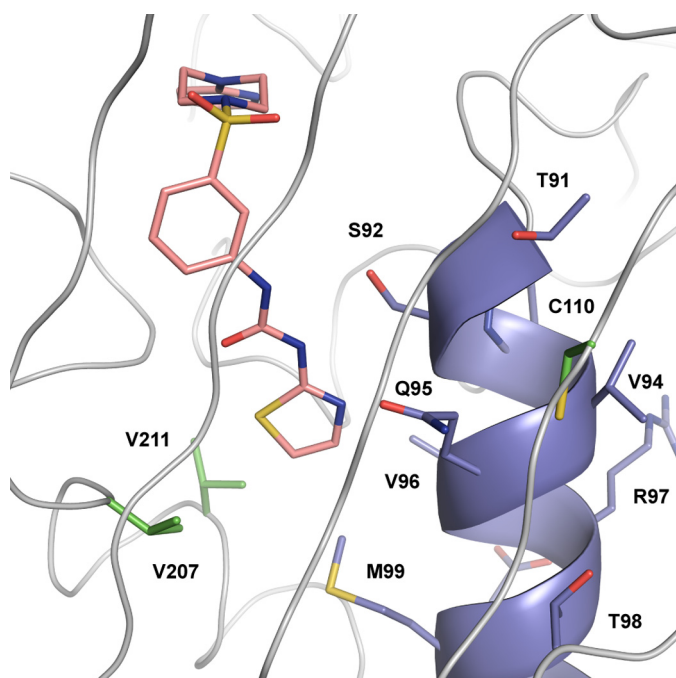

FIGURE 7. **Resistance mutations.** *E. coli* resistance mutants have been mapped onto the crystal structure of *P. aeruginosa* PheRS in complex with compound **1a**. Residues Cys-110, Val-207, and Val-211 are shown as *green sticks* and labeled. The helix that forms an integral part of the phenylalanyl-adenylate binding pocket is colored *purple*. Compound **1a** is shown with *pink* carbon atoms, *blue* nitrogen atoms, *red* oxygen atoms, and *yellow* sulfur atoms.

P. aeruginosa PheRS structure) would introduce negatively charged side chains into the binding pocket that would significantly change its hydrophobicity and shape, clearly abolishing inhibitor binding. The third *E. coli* resistance mutation, A189E (C110E in *P. aeruginosa* PheRS), is positioned directly in front of the α-helix that forms an integral component of the phenylalanyl-adenylate binding pocket (Fig. 7). The presence of a glutamate residue at this position would impact the integrity of the phenylalanyl-adenylate binding pocket.

Viable *E. coli* resistance mutations could be isolated because compound **1a** extends into the auxiliary hydrophobic pocket, which is not involved in phenylalanine binding or the aminoacylation of tRNA[Phe]. Interestingly, resistance to toxic halogenated phenylalanine analogs was identified by mutating residue Ala-226 of *P. aeruginosa* PheS, which is positioned just below the phenylalanine molecule (47).

The phenylalanine binding site of PheRS can accommodate the binding and aminoacylation of other amino acids, including tyrosine. To minimize the misincorporation rate, PheRS evolved an editing domain to catalyze the hydrolysis of tyrosinyl-adenylate, instead of evolving a smaller binding pocket with increased selectivity. Although this structural feature holds promise for the design of proteins with novel functionality (48), it is a liability for drug discovery. First, the hydrophobicity of the pocket results in identification of chemical starting points with poor physicochemical properties, including the phenyl-thiazolylurea-sulfonamides and the scaffolds described here. Second, given the abundance of structurally related chemical compounds in our corporate compound collection, those compounds with more attractive physicochemical properties (potentially binding in the more hydrophilic ATP binding site of PheRS) would be assigned a lower relative ranking for resynthesis and characterization given their reduced biochemical potencies. Third, resistance mutations positioned within the auxiliary binding site occurred at a rate of 10^{-8}–10^{-7}. This observation suggests that PheRS inhibitors would be susceptible to the rapid development of clinical resistance, as observed for inhibitor AN3365/GSK2251052, which inactivates the nonessential editing function of LeuRS (49).[4] This liability is amplified by high bacterial growth rates; similar pockets have been successfully exploited in other therapeutic areas (50).

Silver (51) previously highlighted the clinical resistance risk associated with single gene target inhibitors and suggested that despite this liability, they may have clinical utility. Because there is no functional redundancy for PheRS (unlike, for example, peptide deformylase (52)), alternative lead generation approaches could be pursued. An enzymatic screen could be performed using the resistance mutants described here, followed by hit confirmation using the wild-type enzyme. This is likely to lead to the identification of inhibitors that span phenylalanine and ATP binding sites. We also envision the design of substrate or transition state analogs and their potential utility in a screening cascade (53). Irrespective of the approach taken, inhibitor binding in the auxiliary pocket should be avoided, thus ensuring mutations would be rendered unviable by pre-

---

[4] ClinicalTrials.gov (February 13, 2014) GSK2251052 in complicated urinary tract infection.

venting binding of both inhibitor and substrate to PheRS, thereby minimizing the rate of resistance.

REFERENCES

1. Raczniak, G., Ibba, M., and Söll, D. (2001) Genomics-based identification of targets in pathogenic bacteria for potential therapeutic and diagnostic use. *Toxicology* **160,** 181–189

2. Gentry, D. R., Ingraham, K. A., Stanhope, M. J., Rittenhouse, S., Jarvest, R. L., O'Hanlon, P. J., Brown, J. R., and Holmes, D. J. (2003) Variable sensitivity to bacterial methionyl-tRNA synthetase inhibitors reveals subpopulations of *Streptococcus pneumoniae* with two distinct methionyl-tRNA synthetase genes. *Antimicrob. Agents Chemother.* **47,** 1784–1789

3. Seah, C., Alexander, D. C., Louie, L., Simor, A., Low, D. E., Longtin, J., and Melano, R. G. (2012) MupB, a new high-level mupirocin resistance mechanism in *Staphylococcus aureus. Antimicrob. Agents Chemother.* **56,** 1916–1920

4. Eriani, G., Delarue, M., Poch, O., Gangloff, J., and Moras, D. (1990) Partition of tRNA synthetases into two classes based on mutually exclusive sets of sequence motifs. *Nature* **347,** 203–206

5. Cusack, S. (1995) Eleven down and nine to go. *Nat. Struct. Biol.* **2,** 824–831

6. Arnez, J. G., and Moras, D. (1997) Structural and functional considerations of the aminoacylation reaction. *Trends Biochem. Sci.* **22,** 211–216

7. Khodyreva, S. N., Moor, N. A., Ankilova, V. N., and Lavrik, O. I. (1985) Phenylalanyl-tRNA synthetase from *E. coli* MRE-600: analysis of the active site distribution on the enzyme subunits by affinity labeling. *Biochim. Biophys. Acta* **830,** 206–212

8. Mosyak, L., Reshetnikova, L., Goldgur, Y., Delarue, M., and Safro, M. G. (1995) Structure of phenylalanyl-tRNA synthetase from *Thermus thermophilus. Nat. Struct. Biol.* **2,** 537–547

9. Fraser, T. H., and Rich, A. (1975) Amino acids are not all initially attached to the same position on transfer RNA molecules. *Proc. Natl. Acad. Sci. U.S.A.* **72,** 3044–3048

10. Sprinzl, M., and Cramer, F. (1975) Site of aminoacylation of tRNAs from *Escherichia coli* with respect to the 2'- or 3'-hydroxyl group of the terminal adenosine. *Proc. Natl. Acad. Sci. U.S.A.* **72,** 3049–3053

11. Baltzinger, M., and Holler, E. (1982) Catalytic mechanism of phenylalanyl-tRNA synthetase of *Escherichia coli* K10. Conformational change and tRNA^{Phe} phenylalanylation are concerted. *Biochemistry* **21,** 2467–2476

12. Kotik-Kogan, O., Moor, N., Tworowski, D., and Safro M. (2005) Structural basis for discrimination of L-phenylalanine from L-tyrosine by phenylalanyl-tRNA synthetase. *Structure* **13,** 1799–1807

13. Rodova, M., Ankilova, V., and Safro, M. G. (1999) Human phenylalanyl-tRNA synthetase: cloning, characterization of the deduced amino acid sequences in terms of the structural domains and coordinately regulated expression of the alpha and beta subunits in chronic myeloid leukemia cells. *Biochem. Biophys. Res. Commun.* **255,** 765–773

14. Sanni, A., Walter, P., Boulanger, Y., Ebel, J. P., and Fasiolo, F. (1991) Evolution of aminoacyl-tRNA synthetase quaternary structure and activity: *Saccharomyces cerevisiae* mitochondrial phenylalanyl-tRNA synthetase. *Proc. Natl. Acad. Sci. U.S.A.* **88,** 8387–8391

15. Yu, X. Y., Finn, J., Hill, J. M., Wang, Z. G., Keith, D., Silverman, J., and Oliver, N. (2004) A series of spirocyclic analogues as potent inhibitors of bacterial phenylalanyl-tRNA synthetases. *Bioorg. Med. Chem. Lett.* **14,** 1339–1342

16. Yu, X. Y., Finn, J., Hill, J. M., Wang, Z. G., Keith, D., Silverman, J., and Oliver, N. (2004) A series of heterocyclic inhibitors of bacterial phenylalanyl-tRNA synthetases with antibacterial activity. *Bioorg. Med. Chem. Lett.* **14,** 1343–1346

17. Jarvest, R. L., Erskine, S. G., Forrest, A. K., Fosberry, A. P., Hibbs, M. J.,

18. Jones, J. J., O'Hanlon, P. J., Sheppard, R. J., and Worby, A. (2005) Discovery and optimisation of potent, selective, ethanolamine inhibitors of bacterial phenylalanyl tRNA synthetase. *Bioorg. Med. Chem. Lett.* **15,** 2305–2309

18. Montgomery, J. I., Toogood, P. L., Hutchings, K. M., Liu, J., Narasimhan, L., Braden T., Dermyer, M. R., Kulynych, A. D., Smith, Y. D., Warmus, J. S., and Taylor, C. (2009) Discovery and SAR of benzyl phenyl ethers as inhibitors of bacterial phenylalanyl-tRNA synthetase. *Bioorg. Med. Chem. Lett.* **19,** 665–669

19. Beyer, D., Kroll, H. P., Endermann, R., Schiffer, G., Siegel, S., Bauser, M., Pohlmann, J., Brands, M., Ziegelbauer, K., Haebich, D., Eymann, C., and Brötz-Oesterhelt, H. (2004) New class of bacterial phenylalanyl-tRNA synthetase inhibitors with high potency and broad-spectrum activity. *Antimicrob. Agents Chemother.* **48,** 525–532

20. Buurman, E. T., Johnson, K. D., Kelly, R. K., and MacCormack, K. (2006) Different modes of action of naphthyridones in Gram-positive and Gram-negative bacteria. *Antimicrob. Agents Chemother.* **50,** 385–387

21. Kreiswirth, B. N., Löfdahl, S., Betley, M. J., O'Reilly, M., Schlievert, P. M., Bergdoll, M. S., Novick, R. P. (1983) The toxic shock syndrome exotoxin structural gene is not detectably transmitted by a prophage. *Nature* **305,** 709–712

22. Masuda, N., Sakagawa, E., Ohya, S., Gotoh, N., Tsujimoto, H., Nishino, T. (2000) Substrate specificities of MexAB-OprM, MexCD-OprJ, and MexXY-oprM efflux pumps in *Pseudomonas aeruginosa. Antimicrob. Agents Chemother.* **44,** 3322–3327

23. Clinical and Laboratory Standards Institute (2009) *Methods for Dilution Antimicrobial Susceptibility Tests for Bacteria That Grow Aerobically: Approved Standard,* 9th Ed., M07-A8, Vol. 29, No. 2. Clinical and Laboratory Standards Institute, Wayne, PA.

24. Sambrook, J., Russell, D. W. (2001) *Molecular Cloning: A Laboratory Manual,* 2nd Ed., pp A2.2, Cold Spring Harbor, NY

25. Hilliard, J. J., Goldschmidt, R. M., Licata, L., Baum, E. Z., and Bush K. (1999) Multiple mechanisms of action for inhibitors of histidine protein kinases from bacterial two-component systems. *Antimicrob. Agents Chemother.* **43,** 1693–1699

26. Buurman, E. T., Andrews, B., Gao, N., Hu, J., Keating, T. A., Lahiri, S., Otterbein, L. R., Patten, A. D., Stokes, S. S., Shapiro, A. B. (2011) *In vitro* validation of acetyltransferase activity of GlmU as an antibacterial target in *Haemophilus influenzae. J. Biol. Chem.* **286,** 40734–40742

27. Evdokimov, A. G., Mekel, M., Hutchings, K., Narasimhan, L., Holler, T., McGrath, T., Beattie, B., Fauman, E., Yan, C., Heaslet, H., Walter, R., Finzel, B., Ohren, J., McConnell, P., Braden, T., Sun, F., Spessard, C., Banotai, C., Al-Kassim, L., Ma, W., Wengender, P., Kole, D., Garceau, N., Toogood, P., and Liu, J. (2008) Rational protein engineering in action: the first crystal structure of a phenylalanine tRNA synthetase from *Staphylococcus haemolyticus. J. Struct. Biol.* **162,** 152–169

28. Kabsch, W. (2010) XDS. *Acta Crystallogr. D Biol. Crystallogr.* **66,** 125–132

29. Collaborative Computational Project, Number 4 (1994) The CCP4 suite: programs for protein crystallography. *Acta Crystallogr. D* **50,** 760–763

30. Vonrhein, C., Flensburg, C., Keller, P., Sharff, A., Smart, O., Paciorek, W., Womack, T., and Bricogne, G. (2011) Data processing and analysis with the autoPROC toolbox. *Acta Crystallogr. D* **67,** 293–302

31. Otwinowski, Z., and Minor, W. (1997) Processing of x-ray diffraction data collected in oscillation mode. *Methods Enzymol.* **276,** 307–326

32. Vagin, A., and Teplyakov, A. (1997) MOLREP: an automated program for molecular replacement. *J. Appl. Crystallogr.* **30,** 1022–1025

33. Emsley, P., Lohkamp, B., Scott, W. G., and Cowtan, K. (2010) Features and development of Coot. *Acta Crystallogr. D* **66,** 486–501

34. Bricogne, G., Blanc, E., Brandl, M., Flensburg, C., Keller, P., Paciorek, W., Roversi, P., Smart, O. S., Vonrhein, C., and Womack, T. O. (2009) *BUSTER,* version 2.8.0, Global Phasing Ltd., Cambridge, UK

35. Dalvit, C., Fogliatto, G., Stewart, A., Veronesi, M., and Stockman, B. (2001) WaterLOGSY as a method for primary NMR screening: practical aspects and range of applicability. *J. Biomol. NMR* **21,** 349–359

36. Scott, K. S., Keeler, J., Hwang, T. L., and Shaka A. J. (1995) Excitation sculpting in high-resolution nuclear magnetic resonance spectroscopy: application to selective NOE experiments. *J. Am. Chem. Soc.* **117,** 4199-4200

37. Reck, F., Alm, R., Brassil, P., Newman, J., Dejonge, B., Eyermann, C. J.,

Breault, G., Breen, J., Comita-Prevoir, J., Cronin, M., Davis, H., Ehmann, D., Galullo, V., Geng, B., Grebe, T., Morningstar, M., Walker, P., Hayter, B., and Fisher, S. (2011) Novel *N*-linked aminopiperidine inhibitors of bacterial topoisomerase type II: broad spectrum antibacterial agents with reduced hERG activity. *J. Med. Chem.* **54,** 7834–7847

38. Buurman, E. T., Foulk, M. A., Gao, N., Laganas, V. A., McKinney, D. C., Moustakas, D. T., Rose, J. A., Shapiro, A. B., and Fleming, P. R. (2012) Novel rapidly diversifiable antimicrobial RNA polymerase switch region inhibitors with confirmed mode of action in *Haemophilus influenzae. J. Bacteriol.* **194,** 5504–5512

39. Artsimovitch, I., Patlan, V., Sekine, S., Vassylyeva, M. N., Hosaka, T., Ochi, K., Yokoyama, S., and Vassylyev, D. G. (2004) Structural basis for transcription regulation by alarmone ppGpp. *Cell* **117,** 299–310

40. Wendrich, T. M., Blaha, G., Wilson, D. N., Marahiel, M. A., and Nierhaus, K. H. (2002) Dissection of the mechanism for the stringent factor RelA. *Mol. Cell* **10,** 779–788

41. Ibba, M., Kast, P., and Hennecke, H. (1994) Substrate specificity is determined by amino acid binding pocket size in *Escherichia coli* phenylalanyl-tRNA synthetase. *Biochemistry* **33,** 7107–7112

42. Mermershtain, I., Finarov, I., Klipcan, L., Kessler, N., Rozenberg, H., and Safro, M. G. (2011) Idiosyncrasy and identity in the prokaryotic Phe-system: crystal structure of *E. coli* phenylalanyl-tRNA synthetase complexed with phenylalanine and AMP. *Protein Sci.* **20,** 160–167

43. Moor, N., Kotik-Kogan, O., Tworowski, D., Sukhanova M., and Safro, M. (2006) The crystal structure of the ternary complex of phenylalanyl-tRNA synthetase with tRNAPhe and a phenylalanyl-adenylate analogue reveals a conformational switch of the CCA end. *Biochemistry* **45,** 10572–10583

44. Reshetnikova, L., Moor, N., Lavrik, O., and Vassylyev, D. G. (1999) Crystal structures of phenylalanyl-tRNA synthetase complexed with phenylalanine and a phenylalanyl-adenylate analogue. *J. Mol. Biol.* **287,** 555–568

45. Hughes, J., and Mellows, G. (1978) Inhibition of isoleucyl-transfer ribonucleic acid synthetase in *Escherichia coli* by pseudomonic acid. *Biochem. J.* **176,** 305–318

46. Payne, D. J., Gwynn, M. N., Holmes, D. J., and Pompliano, D. L. (2007) Drugs for bad bugs: confronting the challenges of antibacterial discovery. *Nat. Rev. Drug Discov.* **6,** 29–40

47. Kast, P., and Hennecke, H. (1991) Amino acid substrate specificity of *Escherichia coli* phenylalanyl-tRNA synthetase altered by distinct mutations. *J. Mol. Biol.* **222,** 99–124

48. Liu, C. C., and Schultz, P. G. (2010) Adding new chemistries to the genetic code. *Annu. Rev. Biochem.* **79,** 413–444

49. Hernandez, V., Crépin, T., Palencia, A., Cusack, S., Akama, T., Baker, S. J., Bu, W., Feng, L., Freund, Y. R., Liu, L., Meewan, M., Mohan, M., Mao, W., Rock, F. L., Sexton, H., Sheoran, A., Zhang, Y., Zhang, Y. K., Zhou, Y., Nieman, J. A., Anugula, M. R., Keramane el, M., Savariraj, K., Reddy, D. S., Sharma, R., Subedi, R., Singh, R., O'Leary, A., Simon, N. L., De Marsh, P. L., Mushtaq, S., Warner, M., Livermore, D. M., Alley, M. R., and Plattner, J. J. (2013) Discovery of a novel class of boron-based antibacterials with activity against Gram-negative bacteria. *Antimicrob. Agents Chemother.* **57,** 1394–1403

50. Kurumbail, R. G., Stevens, A. M., Gierse, J. K., McDonald, J. J., Stegeman, R. A., Pak, J. Y., Gildehaus, D., Miyashiro, J. M., Penning, T. D., Seibert, K., Isakson, P. C., and Stallings, W. C. (1996) Structural basis for selective inhibition of cyclooxygenase-2 by anti-inflammatory agents. *Nature* **384,** 644–648

51. Silver, L. L. (2007) Multi-targeting by monotherapeutic antibacterials. *Nat. Rev. Drug Discov.* **6,** 41–55

52. Margolis, P. S., Hackbarth, C. J., Young, D. C., Wang, W., Chen, D., Yuan, Z., White, R., and Trias, J. (2000) Peptide deformylase in *Staphylococcus aureus*: resistance to inhibition is mediated by mutations in the formyltransferase gene. *Antimicrob. Agents Chemother.* **44,** 1825–1831

53. Schramm, V. L. (2013) Transition states, analogues, and drug development. *ACS Chem. Biol.* **8,** 71–81